Supporting Information

Directed Motion of an Impinging Water Droplet — Seesaw Effect

Shun Wang,[†a,b] Hailong Li,[†c] Hu Duan,[†a] Yingtao Cui,[†a] Heng Sun,[a] Mengjiao Zhang,[a] Xianfu Zheng,[a] Meirong Song,*[a] He Li,*[a] Zhichao Dong,*[b] Hang Ding*[c] and Lei Jiang[b]

[a] College of Science and College of Mechanical & Electrical Engineering, Henan Agricultural University, Zhengzhou, Henan 450002, P. R. China

[b] CAS Key Laboratory of Bio-inspired Materials and Interfacial Science, Technical Institute of Physics and Chemistry, Chinese Academy of Sciences Future Technology College, University of Chinese Academy of Sciences, Chinese Academy of Sciences, Beijing 100190, P. R. China

[c] Department of Modern Mechanics, University of Science and Technology of China, Anhui 230022, P. R. China

E-mail: smr770505@iccas.ac.cn (M. S.), chungbuk@163.com (H. L.), dongzhichao@iccas.ac.cn (Z. D.), hding@ustc.edu.cn (H. D.).

Supplement numerical simulation method: Numerical method

Fig. S1 The directed motion of a droplet impinging upon a superhydrophobic interface with four different degrees of roughness.

Fig. S2 Effect of the impact position of the droplet on the deviation factor.

Fig. S3 Decrease in displacement and breaking of the impacting droplet due to ridge effect.

Fig. S4 Correlation between the deviation factor and the structural dimension on three typical heterogeneous superhydrophobic surfaces.

Fig. S5 Spreading edge positions (leftmost and rightmost, indicated by the linkage between the two red dots in Fig. 3).

Fig. S6 Horizontal lines linking the spreading edge positions (leftmost and rightmost) of an impinging droplet on a homogeneous superhydrophobic surface.

Fig. S7 Simulated dynamic impacts on *H*-flat/*L*-flat (a), Cone/*L*-flat (b), and *H*-flat/Cone (c) interfaces.

Fig. S8 Comparisons of momentum, mass ratio and movement speed of the left and right parts of the impinging droplet divided by the three interfaces.

Movie S1 Difference between hydrophobic surfaces with low and high adhesive properties with the same contact angle of approximately 140°. The water droplet easily slides off the macro-structured surface, contrary to the highly adhesive hydrophobic surface upon which the water droplet hangs without falling.

Movie S2 Directional bouncing behaviour on a superhydrophobic interface with four different degrees of roughness. The water droplet finally bounces to the area with the lowest roughness. Impact velocity: 0.51 m s^{-1}.

Movie S3 Directional bouncing behaviour on *H*-flat/cone superhydrophobic interface.

Movie S4 Non-directional bouncing behaviour on flat and conical surfaces. Impact velocity: 0.51 m s^{-1}.

Movie S5 Directional bouncing behaviour of the droplet after impacting *H*-flat/*L*-flat and Cone/*L*-flat superhydrophobic interface. Impact velocity: 0.51 m s^{-1}.

Movie S6 Directional bouncing behaviour of the capsule impacting *H*-flat/*L*-flat and Cone/*L*-flat superhydrophobic interface. Impact velocity: 0.51 m s^{-1}.

Movie S7 Simulated dynamic impacts on *H*-flat/*L*-flat (a), Cone/*L*-flat (b), and *H*-flat/Cone (c) interfaces. Impact velocity: 0.51 m s^{-1}.

Movie S8 Rotational behaviour of impacting droplets on a superhydrophobic/hydrophilic interface. (a) One-way rotational behaviour of a droplet impacting upon a superhydrophobic/hydrophilic interface. Impact velocity: 0.82 m s^{-1}. (b) Tiny droplet ejected during the rotational process at higher impact velocity (1.48 m s^{-1}). (c) Anti-gravity pendulum impact dynamics showing double-way rotation behaviour on superhydrophobic/hydrophilic/superhydrophobic interfaces. Impact velocity: 1.08 m s^{-1}.

Movie S9 Adjusting the direction in which a droplet bounces by tuning the inclined angle to act as a tri-directional switch. (a) Bouncing to the left at an angle of lower inclination. (b) Landing at the position of initial impact at the critical angle. (d) Bouncing to the right at an angle of higher inclination. Impact velocity: 0.51 m s^{-1}.

Supplement numerical simulation method

Numerical methods

We simulated the impact of a droplet with the three gradient inerfaces using a three dimensional diffuse-interface immersed-boundary (DIIB) method.[1-3] The liquid-gas interface is represented by the volume fraction of the liquid, C_L, the evolution of which can be tracked by the Cahn-Hillard equation,

$$\frac{\partial C_L}{\partial t} + \nabla\cdot(uC_L) = \frac{1}{P_e}\nabla^2\psi \tag{1}$$

where u is the flow velocity and ψ is the chemical potential,

$$\psi = C_L^3 - 1.5C_L^2 + 0.5C_L - C_LC_S(1 - C_L - C_S) - Cn^2\nabla^2C_L \tag{2}$$

In the present study, the Cahn number Cn is set to $0.75\Delta x/D$ and the Pelect number Pe to $1/Cn$, where Δx is the mesh size. The curved parts of the substrate are represented by the volume fraction of the solid, C_S.

The three-dimensional flow is obtained by solving 3D incompressible Naiver-Stokes equations, whose dimensionless forms are,

$$\rho\left(\frac{\partial u}{\partial t} + u\cdot\nabla u\right) = -\nabla P + \frac{1}{R_e}\nabla\cdot\left[\mu\left(\nabla u + \nabla u^T\right)\right] + \frac{f_s}{W_e} + \frac{f_g}{F_r}) \tag{3}$$

$$\nabla\cdot\mathbf{u} = 0, \tag{4}$$

where the density and viscosity are $\rho = C_L\rho_L + (1-C_L)\rho_G$ and $\mu = C_L\mu_L + (1-C_L)\mu_G$, respectively. The subscripts L and G represent liquid and gas, respectively. $\mathbf{f}_S$ and $\mathbf{f}_g$ denote the surface tension force and gravity force. The impact velocity v and the diameter of the droplet diameter D are chosen as the characteristic velocity and length. The corresponding dimensionless numbers are Reynolds number $Re = \rho vD/\mu$, Weber number $We = \rho v^2D/\sigma$ and Froude number $Fr = v^2/g/D$, where σ is the surface tension force coefficient. To simulate the motion of the CLs, a characteristic moving CL model [3] is employed. The wettability of the droplet is represented by the contact angle θ. Additional details regarding the numerical implementation can be found in refs 2 and 3.

References

1 H. R. Liu, P. Gao and H. Ding, *J. Comput. Phys.*, 2017, **348**, 45-65.
2 H. R. Liu, H. Ran and H. Ding, *J. Comput. Phys.*, 2015, **294**, 484-502.
3 Y. Zhu, H. R. Liu, K. Mu, P. Gao, H. Ding and X. Y. Lu, *J. Fluid Mech.*, 2017, **824**, 484-502.

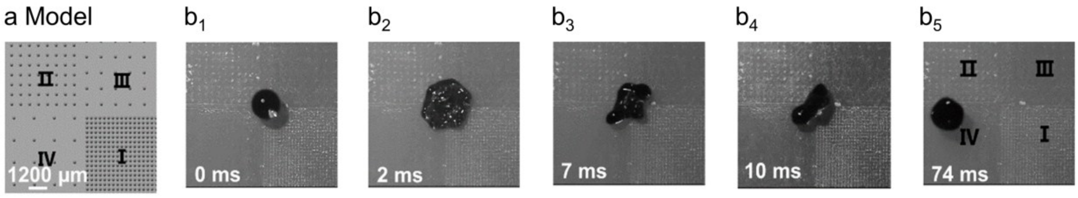

Fig. S1 The directed motion of a droplet impinging upon a superhydrophobic interface with four different degrees of roughness. (a) Four different degrees of roughness on the interface, where I–IV represent areas with a cone spacing of 300, 600, 900, and 1,200 μm, respectively. (b_1–b_5) Directional motion behaviour of the impinging droplet. The droplet eventually lands in area IV, where the cone spacing is the largest and roughness is the lowest.

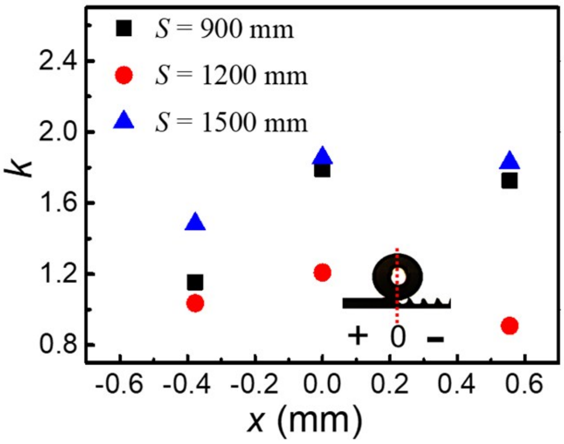

Fig. S2 Effect of the impact position of the droplet on the deviation factor. The deviation factor is largest when the droplet impacts the centre of the interface. Impact velocity: 0.51 m s^{-1}

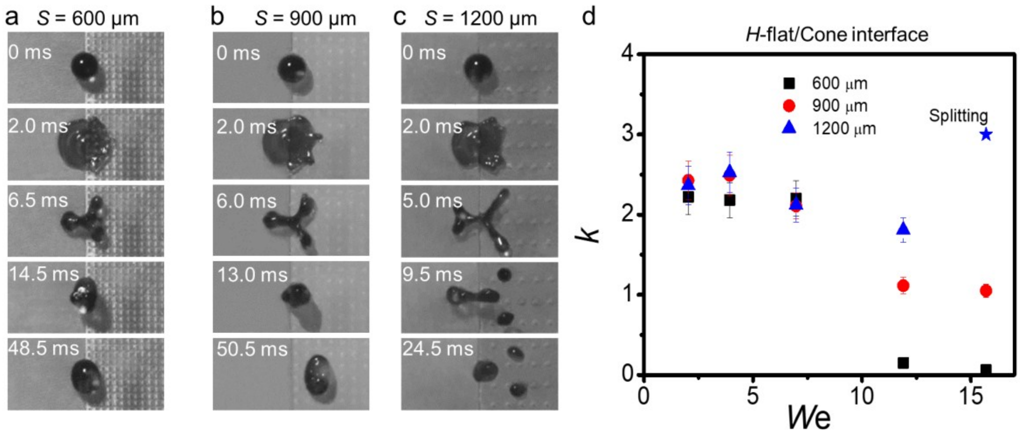

Fig. S3 Decrease in displacement and breaking of the impacting droplet due to ridge effect. (a-c) Impacts on the interface of *H*-flat/Cone with S= 600 μm, 900 μm and 1200 μm at *We* = 15.7, respectively. (d) The decrease in deviation factor with the increase of *We*.

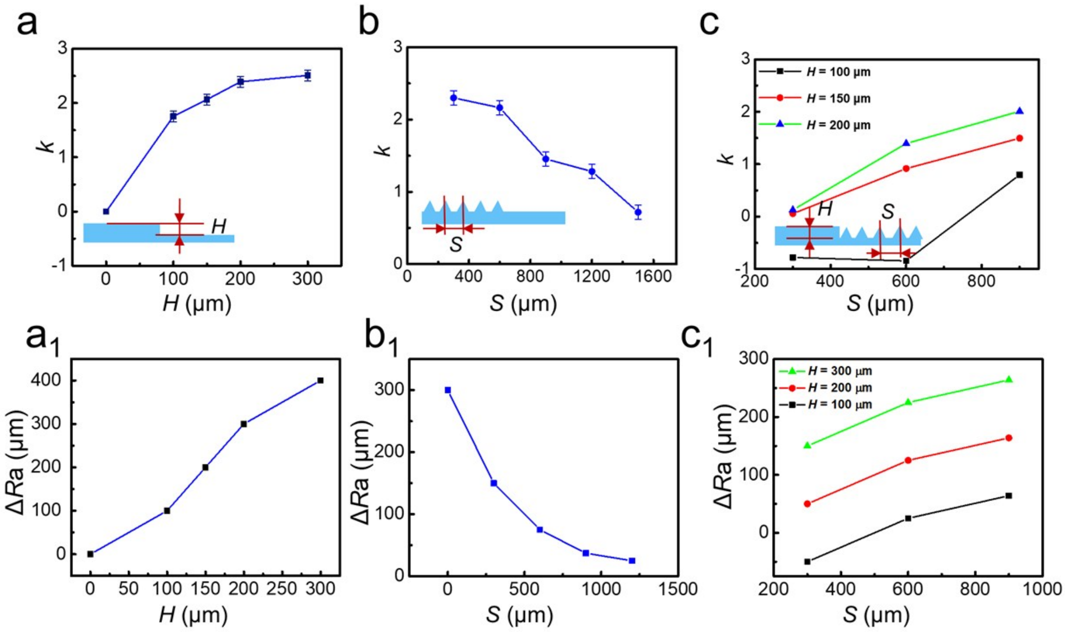

Fig. S4 Correlation between the deviation factor and the structural dimension on three typical heterogeneous superhydrophobic surfaces. The impact velocity of the droplet: 0.51 m s^{-1}. (a) When the droplet impacts the *H*-flat/*L*-flat interface, the deviation factor *k* increases as the height (*H*) of the H-flat surface increases. (a_1) The roughness difference (ΔRa) between *H*-flat and *L*-flat surfaces as a function of *H*. (b) When the droplet impacts the Cone/*L*-flat interface, the deviation factor decreases with increasing cone spacing *S*. (b_1) The roughness difference between Cone and *L*-flat surfaces as a function of *S*. (c) When the droplet impacts the *H*-flat/Cone interface, the deviation factor is related to both the cone spacing *S* and the height *H* of the *H*-flat surface (the lower the value of *H*, the smaller the deviation factor). This factor can even be negative (with *S* ranging from 300 to 600 μm and *H*=100 μm), suggesting that the direction of deviation has changed. (c_1) The roughness difference between *H*-flat and Cone surfaces as a function of *S*.

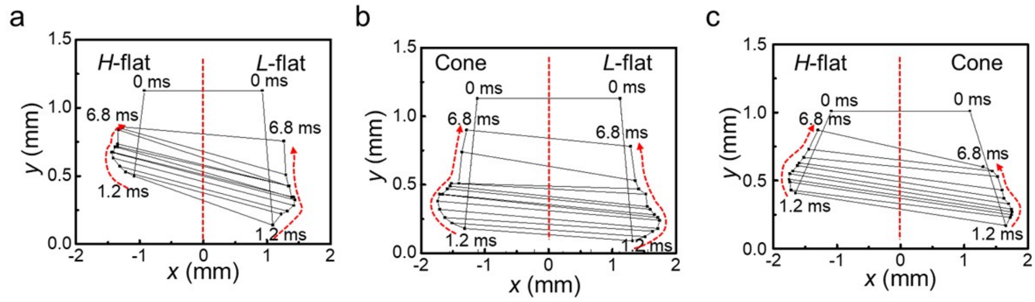

Fig. S5 Spreading edge positions (leftmost and rightmost, indicated by the linkage between the two red dots in Fig. 3). (a) For impact on *H*-flat/*L*-flat interface. (b) For impact on Cone/*L*-flat interface. (c) For impact on *H*-flat/Cone interface.

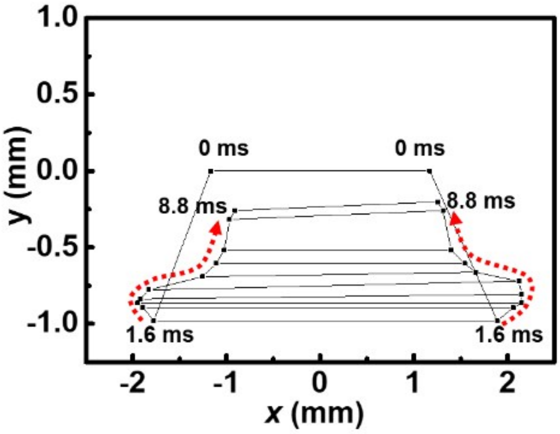

Fig. S6 Horizontal lines linking the spreading edge positions (leftmost and rightmost) of an impinging droplet on a homogeneous superhydrophobic surface

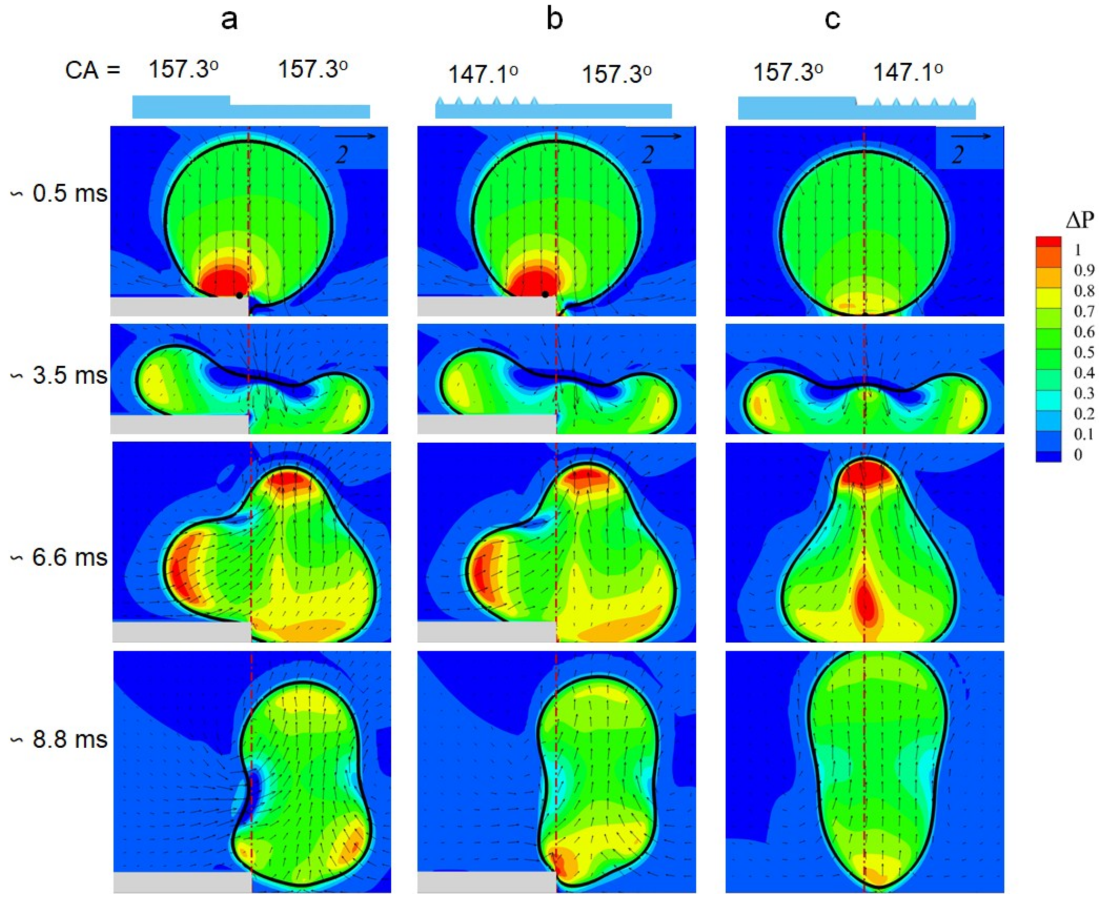

Fig. S7 Simulated dynamic impacts on *H*-flat/*L*-flat (a), Cone/*L*-flat (b), and *H*-flat/Cone (c) interfaces. Here, $\Delta P = \frac{P - P_0}{\frac{1}{2}\rho v^2}$, ΔP is the pressure difference between actual pressure (P) and atmospheric pressure (P_0), ρ and v are the density and impact velocity of the impinging droplet, respectively. The impact velocity is 0.51 m s^{-1} and the diameter of droplet is 2.2 mm.

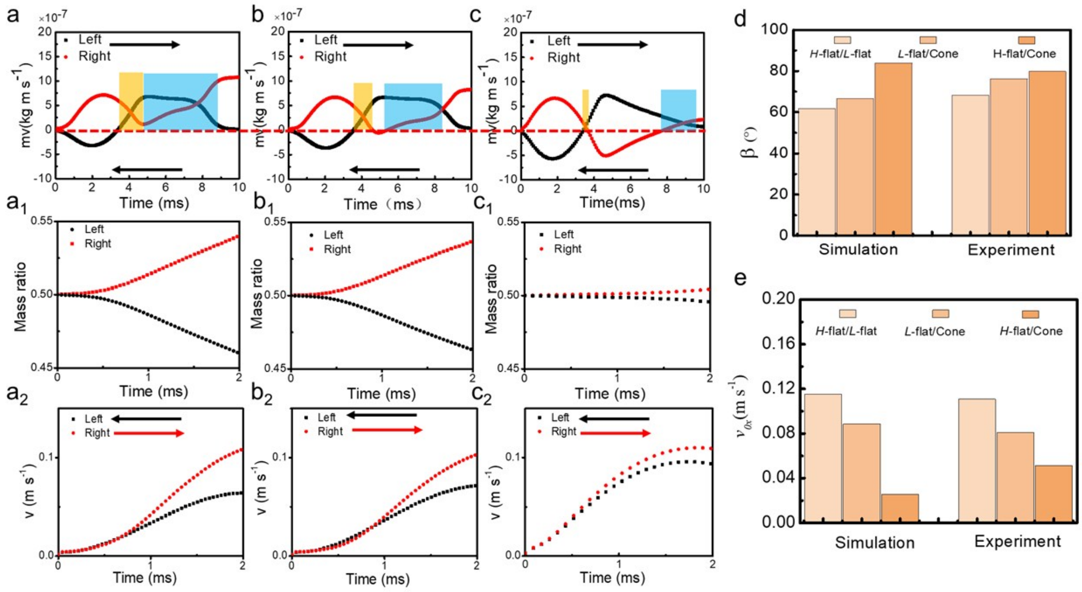

Fig. S8 Comparisons of momentum, mass ratio and movement speed of the left and right parts of the impinging droplets divided by the three interfaces. (a-c) Momentum comparison between left and right parts on *H*-flat/*L*-flat, Cone/*L*-flat and *H*-flat/Cone interfaces, respectively. (a_1-c_1) Mass ratio comparisons on the *H*-flat/*L*-flat, Cone/*L*-flat and *H*-flat/Cone interfaces, respectively. The results show that the mass transport from left to right begins at ～1 ms after the first contact with the substrates. (a_2-c_2) Movement speed comparisons on *H*-flat/*L*-flat, Cone/*L*-flat and *H*-flat/Cone interfaces, respectively. The results show that the movement speed difference begins at ～1 ms after the first contact with the substrates. (d) Comparison of the value of β (at which the droplet takes off) between simulated and experimental results. (e) Comparison of the value of v_{0x} (at which the droplet takes off) between simulated and experimental results.